Mesh-liked Carbon Nanosheets Intercalated into Layered TiO_2 as a Zero-strain Anode for Lithium-ion Storage①

FU Wen-Wu[a, b, c] ZHANG Ming[b, c②] SHEN Zhong-Rong[b, c②]

[a] (*College of Chemistry, Fuzhou University, Fuzhou* 350108, *China*)

[b] (*CAS Key Laboratory of Design and Assembly of Functional Nanostructures, and Fujian Key Laboratory of Nanomaterials, Fujian Institute of Research on the Structure of Matter, Chinese Academy of Sciences, Fuzhou* 350002, *China*)

[c] (*The Laboratory of Rare-earth Functional Materials and Green Energy, Xiamen Institute of Rare Earth Materials, Haixi Institutes, Chinese Academy of Sciences, Xiamen* 361021, *China*)

ABSTRACT Volume change during the insertion/extraction of Li^+ in electrode materials is an important issue to affect the safety and stability of Li-ion batteries. Here, we prepare a near-zero volume change material of COF derived mesh-liked carbon/TiO_2 (MC/TiO_2) composite by using a layered TiO_2 as a template, and a two-dimensional COF material is inserted into the interlayers by the Schiff base polymerization between melamine and terephthalaldehyde, followed by carbonization at 500 ℃ to convert COF to mesh-liked carbon nanosheets. Due to the introduction of mesh-liked carbon nanosheets, the interlayer conductivity of TiO_2 is improved, and the nanocavities in mesh-liked carbon nanosheets provide additional chambers for the insertion/extraction of Li-ions without any change of the interlayer distance. The MC/TiO_2 shows a specific capacity of 472.7 mAh/g at a current density of 0.1 A/g, and good specific capacity retention of 65% remains after 1000 cycles at a current of 1 A/g.

Keywords: layered titanium dioxide, Schiff base reaction, lithium-ion battery, zero-strain anode;

DOI: 10.14102/j.cnki.0254–5861.2011–3054

1 INTRODUCTION

The volume of the electrode materials can be changed in lithium-ion batteries due to the insertion and removal of Li^+[1-3]. For example, silicon-based materials have a volume change of more than 300% and more than 260% for tin-based materials during charge/discharge processes[4]. However, excessive volume expansion would cause the electrode to pulverize and crack, and finally peel off from the current collectors, resulting in sharp attenuation of electrode materials[5-8].

On this basis, titanium-based two-dimensional (2*D*) materials have been widely studied owing to their low volume expansion coefficient[9-13]. Typically, the volume expansion of $Li_4Ti_5O_{12}$ is less than 1%, and the volume expansion of TiO_2 is about 4%[14-18]. However, the theoretical capacity of $Li_4Ti_5O_{12}$ is only 175 mAh/g, which severely limits its application as an anode in high energy density lithium-ion batteries[19, 20]. Besides, TiO_2 exhibits a high theoretical capacity while the diffusion of Li^+ in TiO_2 lattice is limited by its poor electronic and ionic conductivity[21-23]. Therefore, the electrochemical performance of TiO_2 is still very poor at high magnification. Moreover, the polarization resistance at the interface between the active electrode and the electrolyte increases at high current density, leading to an increase in polarization resistance at the high current density[24, 25]. In the process of repeated discharge/charge cycles, the volume expansion of the material is further accelerated, and the material structure is disintegrated, thus hindering the practical application of TiO_2 as an anode material for high-power and high-energy lithium-ion batteries[26-29].

Received 4 December 2020; accepted 15 January 2021

① This project was supported by the National Natural Science Foundation of China (No. 21905282) and the State Key Laboratory of Structural Chemistry, Fujian Institute of Research on the Structure of Matter, Chinese Academy of Sciences (No. 20190016)

② Corresponding authors. Zhang Ming, born in 1985, associate professor. E-mail: mingzhang@fjirsm.ac.cn; Shen Zhong-Rong, born in 1976, professor, E-mail: z-shen@fjirsm.ac.cn

To solve the above problems, we have made a series of composites by introducing graphene into the TiO_2 layers[30-33]. Benefiting from the introduction of graphene-like intercalation with high electronic conductivity, the introduction of the concept of interfacial energy storage doubles the theoretical capacity of TiO_2 (⩾500 mAh/g). The high specific capacity can be attributed to the uniform and continuous carbon layers between TiO_2 layers. This can not only improve the mechanical stability and electrochemical performance of the material, but also provide fast electron transmission and prevent direct contact between TiO_2 and organic electrolyte, avoiding rapid capacity attenuation and safety problems. Although ultra-high capacity has been obtained, the volume expansion reaches 40% during the electrochemical intercalation process of lithium at the first cycle through ex-situ XRD analysis, significantly hindering its practical application in lithium-ion batteries[31].

Therefore, in this work, considering the advantages of interfacial energy storage and improvement of in-layer conductivity, a COF-derived mesh-liked carbon structure is designed to intercalate into layered TiO_2 to replace the carbon nanosheet in our previous work[31]. The materials prepared with this design exhibit the following characteristics: (1) a higher capacity of interface energy storage; (2) the cavitation for Li^+ storage without volume change; (3) the dramatically improved conductivity of internal electrons and the higher rate capability of the material.

2 EXPERIMENTAL

2. 1 Materials

The preparation of layered benzylamine/Ni-substituted TiO_2 (BA/Ni-TiO_2) was reported according to our previous literature[31]. Melamine and terephthalaldehyde were purchased from Aladdin. Ethanol and ethylene glycol were purchased from Sinopharm Chemical Reagent Co., Ltd.

2. 2 Synthesis of the material

2. 2. 1 Synthesis of COF/Ni-TiO_2

First, 0.8 g BA/Ni-TiO_2 and 0.8 g melamine were dissolved into a mixture of 56 mL water and 8 mL ethylene glycol. Next, the solution was refluxed at 100 ℃ for 12 h; afterwards, it was subjected to filtering and washing with excess water, and drying at 60 ℃ overnight. In this process, melamine can replace benzylamine to obtain a melamine intercalated Ni-TiO_2 material called melamine/Ni-TiO_2 (mark as MA/Ni-TiO_2).

Next, 1.0 g MA/Ni-TiO_2 and 1.6 g terephthalaldehyde were put into 60 mL ethylene glycol solution and subjected to ultrasonic treatment; then the mixture was hydrothermally heated at 180 ℃ for 72 h. Afterwards, it was subjected to filtering and washing with excess water, and drying at 60 ℃ overnight. In this process, melamine and terephthalaldehyde are subjected to polymerization reaction form COF by Schiff base reaction between the layers to generate COF/Ni-TiO_2 material.

2. 2. 2 Synthesis of MC/TiO_2

1.0 g COF/Ni-TiO_2 was subjected to carbonization at 500 ℃ for 24 h under nitrogen atmosphere in a tube furnace; then the product was soaked in 20 mL 1 M HCl solution for 24 h to form COF derived mesh-liked carbon/TiO_2 (MC/TiO_2) composite, the product was obtained by washing with a large amount of water and drying it at 60 ℃.

2. 2. 3 Synthesis of mesh-liked carbon nanosheets

1.0 g MC/TiO_2 composite was added into 25 mL 10 wt% HF aqueous solution and subjected to the hydrothermal reaction in a Teflon-lined autoclave at 100 ℃ for 12 h. Then the system was filtered and washed with an excess of water after cooling to room temperature. The final product (mesh-liked carbon nanosheets) was obtained by drying it in a vacuum oven at 60 ℃ overnight.

2. 3 Materials characterization

Powder X-ray diffractometer (XRD, Rigaku Miniflex 600) and Raman spectrometer (LabRAM Aramis spectrometer) were used to analyze the crystal structure and functional group structure of the material. Scanning electron microscope (SEM, Apreo S LoVac) and Transmission Electron Microscope (TEM, FEI Talos 200s microscope equipped with a high-precision EDX spectroscopy detector) were used to characterize the microstructure of the material. Thermogravimetric Analysis (TGA, Mettler-Toledo TGA System) was performed at 5 ℃/min in oxygen from 30 to 800 ℃. For layered material, XRD data with high basal reflections indicate the different interlayer distance of each sample. The interlayer distance of all the samples can be deduced from the reflecting spacing and calculated according to the Bragg's Law with equation $2d\times\sin\theta = n\lambda$ (λ = 0.154 nm).

2. 4 Electrochemical tests

Standard CR2032 coin cells were used to conduct electrochemical performances. The electrode slurry was

prepared by mixing active electrode material (MC/TiO_2 composite), Ketjen Black (ECP-600 JD, Japan Lion Corporation), and polyvinylidene fluoride (Kejing, China) at a ratio of 8/1/1 in N-methyl-2-pyrrolidone (NMP, Dodochem, anhydrous, 99.5%) solvent. Then, the working electrode was prepared by coating the slurry on the copper foil and dried at 120 ℃ overnight. The mass load of the active substance is approximately 1.0 mg/cm^2. The galvanostatic discharge/charge tests were performed on a Neware Test System within the voltage range between 0.05 and 3.0 V. CHI760E electrochemical workstation was used for cyclic voltammetry (CV) and AC impedance (EIS, 0.01 Hz to 100 kHz) tests.

3 RESULTS AND DISCUSSION

3. 1 Synthesis and characterization

The preparation process of the MC/TiO_2 composite material is presented in Fig. 1. BA/Ni-TiO_2 is prepared according to our previous work[31]. Then, melamine is used to exchange benzylamine to obtain MA/Ni-TiO_2 at 100 ℃ for 12 h. Afterwards, terephthalaldehyde is added and reacts with melamine between the layered TiO_2 through the Schiff base reaction at 180 ℃ for 72 h to prepare COF/Ni-TiO_2 composite material. The product is subjected to carbonization at 500 ℃ for 24 h under nitrogen atmosphere to obtain MC/TiO_2 composite.

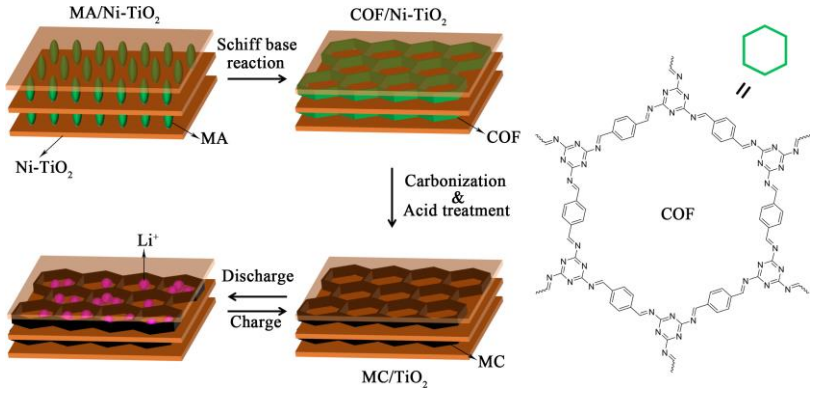

Fig. 1. Schematic illustration of the preparation of MC/TiO_2

The preparation process of the material is characterized by XRD analysis. As indicated in our previous work[31], the interlayer distance of BA/Ni-TiO_2 is expanded from 0.87 to 1.91 nm by the insertion of benzylamine, demonstrating that benzylamine is successfully exchanged into the layered Ni-substituted titanic acid (Ni-TiO_2) under the hydrothermal temperature of 100 ℃. Then, melamine is used to replace benzylamine between the layered Ni-TiO_2, and the layer spacing of MA/Ni-TiO_2 is reduced from 1.91 to 1.31 nm because benzylamine contains only a single amino functional group. Since two layers of benzylamine must be inserted to stabilize the interlayer structure, the amino group on benzylamine is tightly bound to the Ni-TiO_2 layer. However, melamine contains a plurality of amino functional groups. Inserting a layer of melamine molecules can maintain the stability of the structure. Thus, the layer spacing is smaller after being replaced by melamine. After the interlayer Schiff base reaction occurs, the interlayer spacing of COF/Ni-TiO_2 further decreases to only 1.14 nm. Afterwards, the COF/Ni-TiO_2 is subjected to carbonization at 500 ℃ in a nitrogen atmosphere for 24 h. XRD illustrates that the interlayer spacing of the COF-derived mesh-liked carbon/Ni-TiO_2 (MC/Ni-TiO_2) decreases to 0.94 nm due to the formation of a denser sandwich structure (Fig. 2a), resulting in a further decrease in the layer spacing. Therefore, the thickness of the interlayer carbon layer corresponds to approximately one atomic layer by considering the thickness of the Ni-TiO_2 layer. The layer spacing after COF preparation is changed due to the Schiff base reaction, which changes the originally standing melamine into a tiled 2*D* structure. However, the re-change of layer spacing after carbonization may eliminate excess unreacted functional groups such as unreacted complete aldehyde group and an amino group. However, anatase and Ni peaks appear in the XRD patterns in the process of carbonization to form MC/Ni-TiO_2, indicating that the material is reduced owing to the carbothermal reaction, and the phase change occurs in a part of the material at high temperature. Fig. 2b illustrates the Raman spectra of MA/Ni-TiO_2 and COF/Ni-TiO_2 composites. The results indicate that there is no peak after melamine intercalation and the interlayer COF is successfully prepared. Besides,

significant D and G peaks can be observed from the Raman spectra when the material is carbonized, suggesting its successful carbonization. Meanwhile, anatase and rutile peaks can be revealed from the Raman spectra, consistent with the results of XRD analysis. The thermogravimetric curve of MC/TiO_2 composite is exhibited in Fig. 2c. After the removal of Ni elements by acid washing, the weight of the carbon nanosheets inserted between the TiO_2 layers is about 13.7%. The carbon content in MC/TiO_2 composite is much lower than that of the value reported in our previous work. The further elemental analysis demonstrates that the C/N ratio is 1.23, suggesting rich MC/TiO_2 composite in nitrogen. The BET surface area of MC/TiO_2 composite is 11.8 m^3/g, as presented in Fig. 2d. This does not express the pore morphology of the mesh-liked structure, possibly because the dense accumulation cannot reflect the presence of this cavity.

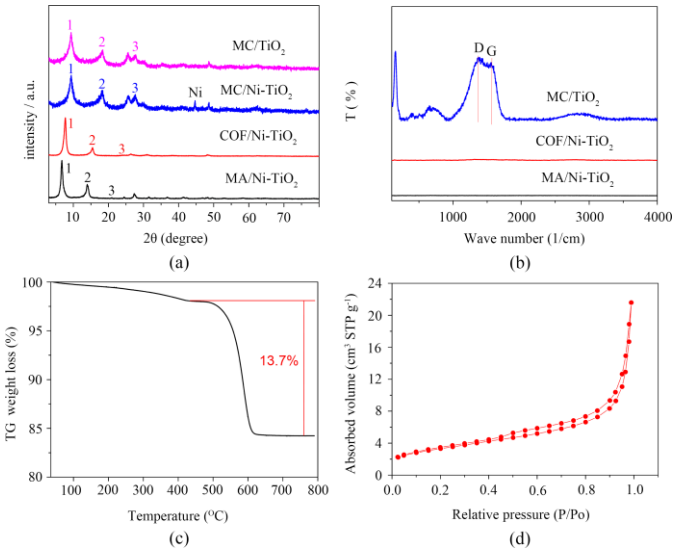

Fig. 2. (a) XRD patterns and (b) Raman spectroscopy of as prepared MA/Ni-TiO_2, COF/Ni–TiO_2, and MC/TiO_2; (c) TGA of MC/TiO_2; (d) BET of MC/TiO_2

The SEM images of MC/TiO_2 at different magnifications are illustrated in Figs. 3a and 3b. It can be observed that the size of the material is about 30～50 microns, indicating a uniform layered structure. The result reveals that the layered structure of the MC/TiO_2 material cannot be damaged during the polymerization and high-temperature carbonization. Compared with the layered structure of Ni–TiO_2 raw material, the whole layer of MC/TiO_2 became thicker. Moreover, its surface is not as smooth as Ni–TiO_2, and the interlayer is densely filled, confirming the interlayer insertion of mesh-liked carbon nanosheet. Fig. 3c exhibits the elements mapping diagrams of the MC/TiO_2 composite. C, N, O, and Ti elements are evenly distributed in the composite. The above results verify that MC/TiO_2 composite is successfully synthesized.

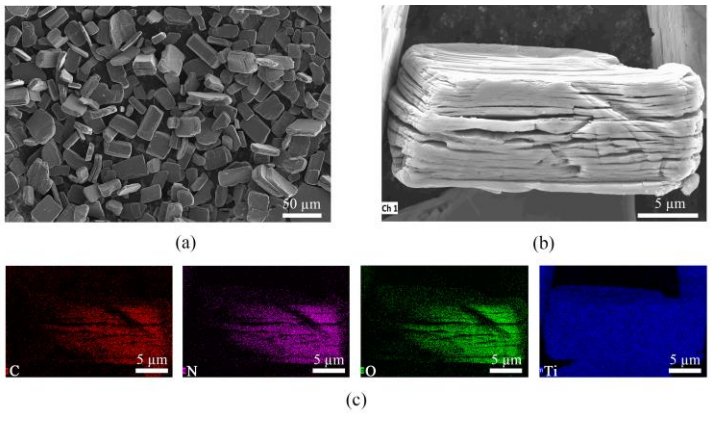

Fig. 3. (a) and (b) SEM images of MC/TiO_2 under different magnifications; (c) EDS mapping diagrams of MC/TiO_2

To further characterize the substances between the TiO_2 layers, HF aqueous solution has been used to wash off the template of layered TiO_2. As presented in Fig. 4, the product after being etched by HF is characterized by XRD, SEM, and TEM. The XRD pattern of mesh-liked carbon nanosheets exhibits a sharp peak at about 27º in Fig. 4a, representing the in-plane structural accumulation of triazine (heptazine) units and the interlayer stacking of carbon nanosheets. The SEM image in Fig. 4b illustrates a 2*D* layered structure with a size of about 30～50 microns, consistent with the size of the MC/TiO_2 composite material, indicating that carbon layers are uniformly inserted between the layered TiO_2. TEM images in Fig. 4c further verify the multi-layer stacking structure of MC/TiO_2. The TEM image of mesh-liked carbon nanosheets at high magnification is displayed in Fig. 4d, revealing the lattice stripes and porous structure of the carbon with partial crystallinity. Meanwhile, the porous structure of the mesh-liked carbon nanosheets indicates the successful preparation of COF between the layered TiO_2.

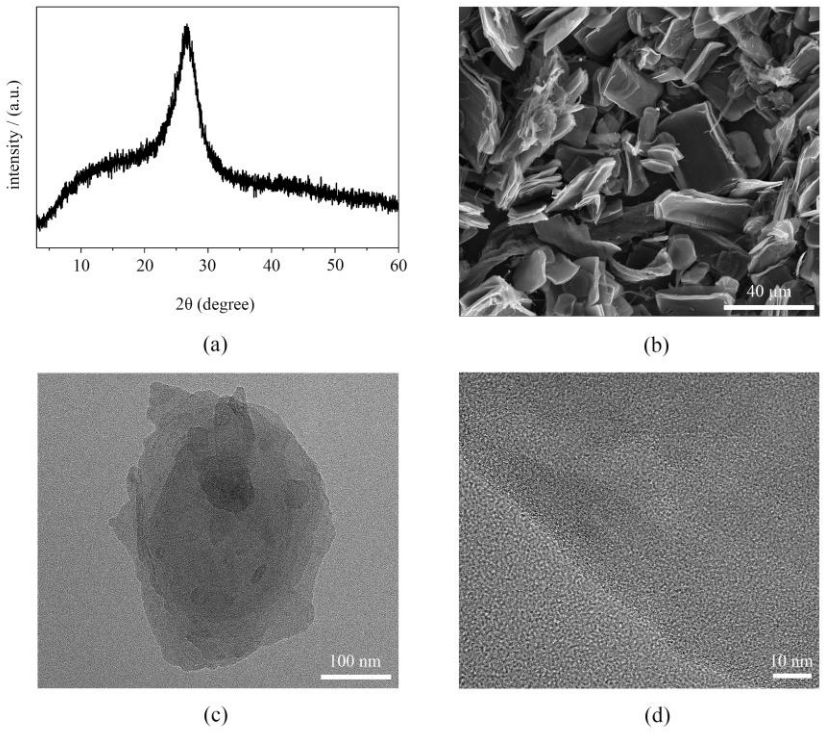

Fig. 4. (a) XRD patterns of mesh-liked carbon nanosheets; (b) SEM image of mesh-liked carbon nanosheets; (c) and (d) TEM images of mesh-liked carbon nanosheets

3. 3 Electrochemistry

Besides, CR2032 coin cells are used to check the electrochemical performances of layered MC/TiO_2 composite material, and Ni–TiO_2 is used for comparison. The specific capacity of layered MC/TiO_2 composites is 472.7 mAh/g at a current density of 0.1 A/g, as demonstrated in Fig. 5a. A high specific capacity of 115.0 mAh/g is achieved at a high current density of 3.2 A/g, which is higher than that of Ni–TiO_2 (35.0 mAh/g) at a high current density of 3.2 A/g. Additionally, the specific capacity of MC/TiO_2 can recover to its original value when the current density is restored to 0.2 A/g. The result indicates that MC/TiO_2 has excellent rate performance and stability as an electrode for lithium-ion batteries. The excellent rate properties of MC/TiO_2 composites can be attributed to the good interfacial contact between TiO_2 and mesh-liked carbon nanosheets. Moreover, these micron-sized transverse structures can provide continuous charge transfer paths, contributing to the enhancement of the conductivity, lithium-ion transmission, and rate capability. Meanwhile, there is no significant voltage platform in the charge-discharge curves of the material (Fig. 5b). Thus, the charge/discharge process of the MC/TiO_2 electrode is almost all pseudocapacitance adsorption/desorption behaviors, and there is almost no significant Li^+ insertion/extraction process.

Fig. 5c presents the electrochemical impedance spectra of coin cells with MC/TiO_2 composite and Ni–TiO_2 electrode. The overall internal resistance and lithium-ion diffusion rate of the MC/TiO_2 are significantly higher compared to Ni–TiO_2 material without the intercalation of carbon nanosheet. The cyclability of the coin cell with MC/TiO_2 as the electrode is characterized by consecutive galvanostatic discharge/charge measurements at a current density of 1 A/g (Fig. 5d). The specific capacity of the material at the first cycle is 253.0 mAh/g, and the specific capacity decreases to 164.4 mAh/g after 1000 charge/discharge cycles. Therefore, the corresponding specific capacity remains 65% of its initial value, and the coulomb efficiency keeps about 100%, demonstrating that the composite material has excellent cycle stability.

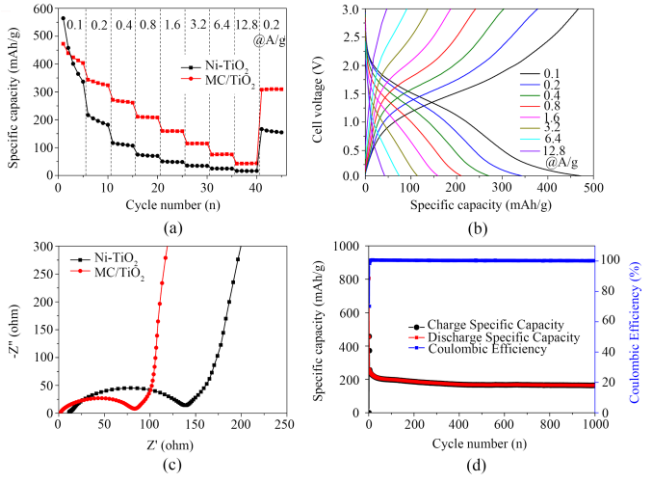

Fig. 5. Comparison of (a) the rate capability of layered Ni–TiO_2 and MC/TiO_2; (c) the representative galvanostatic discharge/charge profiles of MC/TiO_2; (c) impedance spectra of layered Ni–TiO_2 and MC/TiO_2; (d) the cycling performance of the coin cell with MC/TiO_2

The reaction kinetics of MC/TiO_2 is checked by cyclic voltammetry (CV) measurement. A pair of broad cathodic/anodic peaks at 1.23 and 1.75 V can be observed from the representative CV of the MC/TiO_2 at a scan rate of 2 mV/s (Fig. 6a). This can be assigned to the pseudocapacitive lithium storage behavior of MC/TiO_2[34-36]. Meanwhile, a weak peak can be observed at 0.45 V for MC/TiO_2 composite from the first discharge curve, attributed to the formation of solid electrolyte interface (SEI) films on the electrode surfaces and interfaces[37, 38]. However, this peak disappears since the second cycle because the SEI layer can isolate the anodes from the electrolyte, resulting in preventing further decomposition of the electrolyte.

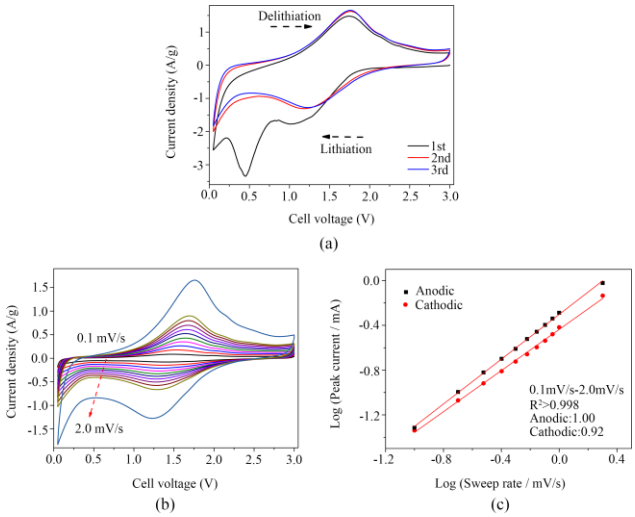

Fig. 6. Kinetic analysis of the MC/TiO_2 electrode. (a) CV curves during initial cycles of 2 mV/s; (b) CV curves at sweep rates from 0.1 to 2 mV/s; (c) Relationship between the peak currents and scan rates in logarithmic format

Moreover, the CV curves of MC/TiO_2 composites in the subsequent two cycles almost overlap, revealing good stability. Additionally, the CV curves at various sweep rates are conducted to evaluate the electrochemical kinetic properties of MC/TiO_2 composite to further verify the lithium storage mechanism. As illustrated in Fig. 6b, all CV curves exhibit similar peak shapes except the corresponding peaks shift during Li^+ insertion/extraction when the scan rate increases from 0.1 to 2.0 mV/s. Nevertheless, the voltage gap between cathodic and anodic peaks increases as the scan rate due to the larger electrode polarization at higher sweep rates.

The charge storage contribution of intercalation/pseudocapacitance can be calculated using the formula $i = av^b$, where i (mA) denotes the peak current, v (mV/s) represents the scan rate, and a and b refer to both adjustable parameters[39-41]. Generally, b = 0.5 and $b \geqslant 1.0$ indicate that the charge storage is contributed by the intercalation and the pseudocapacitor, respectively. As exhibited in Fig. 6c, the b values corresponding to the cathode and anode peaks are 0.92 and 1.0, respectively. Therefore, the charge storage of Li^+ in MC/TiO_2 is a pseudocapacitance process.

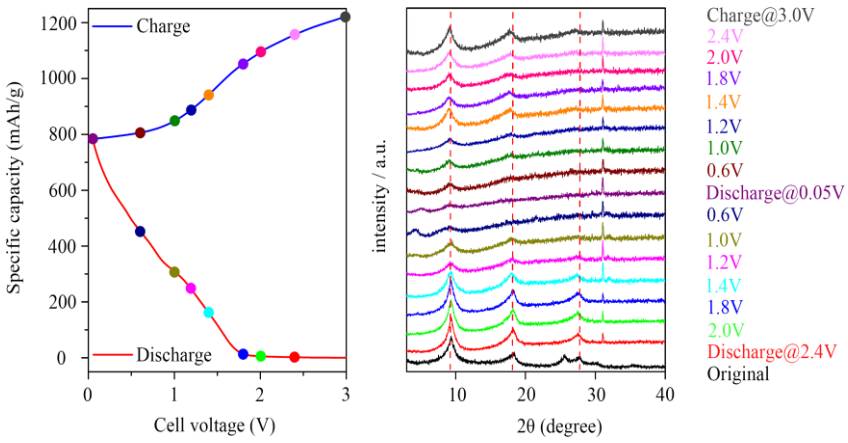

Fig. 7. Ex-situ XRD patterns at different discharged/charged states of MC/TiO_2

Ex-situ XRD is used to characterize the structural changes of MC/TiO_2 during a charge/discharge cycle. As revealed in Fig. 7, the position of the layered peak of MC/TiO_2 at around 9^o exhibits no significant deviation from that of the original material at different charge/discharge stages, quite different from the change of the C/TiO_2 material reported in our previous work[31]. Besides, there is almost near-zero interlayer expansion for the MC/TiO_2 composite in this work. Therefore, the interlayer insertion/extraction of lithium ions is considered to be the main charge storage mechanism for MC/TiO_2 composite (Fig. 1). Generally, the mesh-liked carbon nanosheets prepared between layers can act as a cage, which can store lithium ions during the charging process and release lithium ions during the discharge process. Furthermore, the mesh-liked carbon nanosheets between layers provide large lithium-ion storage space, resulting in near-zero expansion between the layers. Thus, the preferable cycle stability of MC/TiO_2 can be achieved.

4 CONCLUSION

By using 2*D* Ni–TiO_2 as a template, COF is successfully inserted into the layered TiO_2 by Schiff base reaction between melamine and terephthalaldehyde, and a zero-expansion MC/TiO_2 composite material is obtained after the subsequent carbonization treatment. Due to the rapid interfacial pseudocapacitive charge storage behavior between monolayer TiO_2 nanosheets and mesh-liked carbon nanosheets, the composite exhibits a good rate capability. A high specific capacity of 472.7 mAh/g appears at a current density of 0.1 A/g; and a specific capacity of 115 mAh/g remains at a high current density of 3.2 A/g. Moreover, nearly 65.0% of the initial specific capacity can be maintained after 1000 cycles at a current of 1 A/g. Meanwhile, excellent cycle stability is achieved for the resultant MC/TiO_2 composite due to a near-zero volume change during the charge/discharge process. The results show that the MC/TiO_2 composite material is an excellent electrode material for lithium-ion batteries. Besides, the idea of preparing intercalation materials may have potential applications in various energy storage devices and catalysis research.

REFERENCES

(1) Koerver, R.; Zhang, W.; de Biasi, L.; Schweidler, S.; Kondrakov, A. O.; Kolling, S.; Brezesinski, T.; Hartmann, P.; Zeier, W. G.; Janek, J. Chemo-mechanical expansion of lithium electrode materials-on the route to mechanically optimized all-solid-state batteries. *Energy Environ. Sci.* **2018**, 11, 2142–2158.

(2) Winter, M.; Besenhard, J. O. Electrochemical lithiation of tin and tin-based intermetallics and composites. *Electrochim. Acta* **1999**, 45, 31–50.

(3) Zhang, S. L. Chemomechanical modeling of lithiation-induced failure in high-volume-change electrode materials for lithium ion batteries. *NPJ. Comput. Mater.* **2017**, 3, 7–11.

(4) Sun, Y.; Liu, N.; Cui, Y. Promises and challenges of nanomaterials for lithium-based rechargeable batteries. *Nat. Energy* **2016**, 1, 16071–12.

(5) Tong, L.; Wang, P.; Chen, A.; Qiu, F.; Fang, W.; Yang, J.; Wang, C.; Yang, Y. Improved electrochemical performance of binder-free multi-layered silicon/carbon thin film electrode for lithium-ion batteries. *Carbon* **2019**, 153, 592–601.

(6) Su, Q.; Zhang, J.; Wu, Y.; Du, G. Revealing the electrochemical conversion mechanism of porous Co_3O_4 nanoplates in lithium ion battery by *in situ* transmission electron microscopy. *Nano Energy* **2014**, 9, 264–272.

(7) Zhang, H.; Zhao, H.; Khan, M. A.; Zou, W.; Xu, J.; Zhang, L.; Zhang, J. Recent progress in advanced electrode materials, separators and electrolytes for lithium batteries. *J. Mater. Chem. A* **2018**, 6, 20564–20620.

(8) Huang, J. Y.; Zhong, L.; Wang, C. M.; Sullivan, J. P.; Xu, W.; Zhang, L. Q.; Mao, S. X.; Hudak, N. S.; Liu, X. H.; Subramanian, A.; Fan, H.; Qi, L.; Kushima, A.; Li, J. *In situ* observation of the electrochemical lithiation of a single SnO_2 nanowire electrode. *Science* **2010**, 330, 1515–1520.

(9) Fedotov, S. S.; Luchinin, N. D.; Aksyonov, D. A.; Morozov, A. V.; Ryazantsev, S. V.; Gaboardi, M.; Plaisier, J. R.; Stevenson, K. J.; Abakumov, A. M.; Antipov, E. V. Titanium-based potassium-ion battery positive electrode with extraordinarily high redox potential. *Nat. Commun.* **2020**, 11, 1484–11.

(10) Liu, Y.; Yang, Y. Recent progress of TiO_2-based anodes for Li ion batteries. *J. Nanomater.* **2016**, 2016, 8123652–15.

(11) Gardecka, A. J.; Lübke, M.; Armer, C. F.; Ning, D.; Reddy, M. V.; Williams, A. S.; Lowe, A.; Liu, Z.; Parkin, I. P.; Darr, J. A. Nb-doped rutile titanium dioxide nanorods for lithium-ion batteries. *Solid State Sci.* **2018**, 83, 115–121.

(12) Pender, J. P.; Jha, G.; Youn, D. H.; Ziegler, J. M.; Andoni, I.; Choi, E. J.; Heller, A.; Dunn, B. S.; Weiss, P. S.; Penner, R. M.; Mullins, C. B. Electrode degradation in lithium-ion batteries. *ACS Nano* **2020**, 14, 1243–1295.

(13) Li, J.; Huang, J.; Li, J.; Cao, L.; Qi, H.; Cheng, Y. N-doped TiO_2/rGO hybrids as superior Li-ion battery anodes with enhanced Li-ions storage capacity. *J. Alloys Compd.* **2019**, 784, 165–172.

(14) Yi, T. F.; Yang, S. Y.; Xie, Y. Recent advances of $Li_4Ti_5O_{12}$ as a promising next generation anode material for high power lithium-ion batteries. *J. Mater. Chem. A* **2015**, 3, 5750–5777.

(15) Kim, C.; Yu, Y. S.; Moyon, B.; Sirisopanaporn, C.; Richardson, T. J.; Cabana, J. Visualization of the phase propagation within carbon-free $Li_4Ti_5O_{12}$ battery electrodes. *J. Phys. Chem. C* **2016**, 120, 29030–29038.

(16) Yuan, T.; Tan, Z.; Ma, C.; Yang, J.; Ma, Z. F.; Zheng, S. Challenges of spinel $Li_4Ti_5O_{12}$ for lithium-ion battery industrial applications. *Adv. Energy Mat.* **2017**, 7, 1601625–25.

(17) Deng, D. R.; Cui, X. Y.; Wu, Q. H.; Zheng, M. S.; Dong, Q. F. *In-situ* synthesis TiO_2 nanosheets@rGO for ultrafast sodium ion storage at both room and low temperatures. *J. Alloys Compd.* **2020**, 835, 155413–7.

(18) Liu, Q.; Hou, J.; Xu, C.; Chen, Z.; Qin, R.; Liu, H. TiO_2 particles wrapped onto macroporous germanium skeleton as high performance anode for lithium-ion batteries. *Chem. Eng. J.* **2020**, 381, 122649–9.

(19) Sun, X.; Radovanovic, P. V.; Cui, B. Advances in spinel $Li_4Ti_5O_{12}$ anode materials for lithium-ion batteries. *New J. Chem.* **2015**, 39, 38–63.

(20) Zhao, B.; Ran, R.; Liu, M.; Shao, Z. A comprehensive review of $Li_4Ti_5O_{12}$-based electrodes for lithium-ion batteries: the latest advancements and future perspectives. *Mater. Sci. Eng. R.* **2015**, 98, 1–71.

(21) Ghosh, S.; Kiran Kumar, V.; Kumar, S. K.; Biswas, S.; Martha, S. K. An insight of sodium-ion storage, diffusivity into TiO_2 nanoparticles and practical realization to sodium-ion full cell. *Electrochim. Acta* **2019**, 316, 69–78.

(22) Moitzheim, S.; Balder, J. E.; Poodt, P.; Unnikrishnan, S.; De Gendt, S.; Vereecken, P. M. Chlorine doping of amorphous TiO_2 for increased capacity and faster Li^+-ion storage. *Chem. Mater.* **2017**, 29, 10007–10018.

(23) Han, H.; Song, T.; Lee, E. K.; Devadoss, A.; Jeon, Y.; Ha, J.; Chung, Y. C.; Choi, Y. M.; Jung, Y. G.; Paik, U. Dominant factors governing the rate capability of a TiO_2 nanotube anode for high power lithium ion batteries. *ACS Nano* **2012**, 6, 8308–8315.

(24) Wang, Y.; Wu, M.; Zhang, W. F. Preparation and electrochemical characterization of TiO_2 nanowires as an electrode material for lithium-ion batteries.

Electrochim. Acta **2008**, 53, 7863–7868.

(25) Cueto-Gómez, L. F.; Garcia-Gómez, N. A.; Mosqueda, H. A.; Sánchez, E. M. Electrochemical study of TiO_2 modified with silver nanoparticles upon CO_2 reduction. *J. Appl. Electrochem.* **2014**, 44, 675–682.

(26) Farooq, U.; Ahmed, F.; Pervez, S. A.; Rehman, S.; Pope, M. A.; Fichtner, M.; Roberts, E. P. L. A stable TiO_2-graphene nanocomposite anode with high rate capability for lithium-ion batteries. *RSC Adv.* **2020**, 10, 29975–29982.

(27) Bai, Y.; Yan, D.; Yu, C.; Cao, L.; Wang, C.; Zhang, J.; Zhu, H.; Hu, Y. S.; Dai, S.; Lu, J.; Zhang, W. Core-shell Si@TiO_2 nanosphere anode by atomic layer deposition for Li-ion batteries. *J. Power Sources* **2016**, 308, 75–82.

(28) Ren, H.; Yu, R.; Wang, J.; Jin, Q.; Yang, M.; Mao, D.; Kisailus, D.; Zhao, H.; Wang, D. Multishelled TiO_2 hollow microspheres as anodes with superior reversible capacity for lithium ion batteries. *Nano Lett.* **2014**, 14, 6679–6684.

(29) Li, X.; Wu, G.; Liu, X.; Li, W.; Li, M. Orderly integration of porous TiO_2(B) nanosheets into bunchy hierarchical structure for high-rate and ultralong-lifespan lithium-ion batteries. *Nano Energy* **2017**, 31, 1–8.

(30) Li, Y. T.; Chen, M. S.; Cheng, J. F.; Fu, W. W.; Hu, Y. J.; Liu, B. H.; Zhang, M.; Shen, Z. R. Two-dimensional layered ultrathin carbon/TiO_2 nanosheet composites for superior pseudocapacitive lithium storage. *Langmuir* **2020**, 36, 2255–2263.

(31) Fu, W. W.; Li, Y. T.; Chen, M. S.; Hu, Y. J.; Liu, B. H.; Zhang, K.; Zhan, C. Y.; Zhang, M.; Shen, Z. R. An orderly arrangement of layered carbon nanosheet/TiO_2 nanosheet stack with superior artificially interfacial lithium pseudocapacity. *J. Power Sources* **2020**, 468, 228363–7.

(32) Chen, M. S.; Fu, W. W.; Hu, Y. J.; Chen, M. Y.; Chiou, Y. J.; Lin, H. M.; Zhang, M.; Shen, Z. R. Controllable growth of carbon nanosheets in the montmorillonite interlayers for high-rate and stable anode in lithium ion battery. *Nanoscale* **2020**, 12, 16262–16269.

(33) Hu, Y. J.; Li, Y. T.; Cheng, J. F.; Chen, M. S.; Fu, W. W.; Liu, B. H.; Zhang, M.; Shen, Z. R. Intercalation of carbon nanosheet into layered TiO_2 grain for highly interfacial lithium storage. *ACS Appl. Mater. Interfaces* **2020**, 12, 21709–21719.

(34) Cao, M.; Tao, L.; Lv, X.; Bu, Y.; Li, M.; Yin, H.; Zhu, M.; Zhong, Z.; Shen, Y.; Wang, M. Phosphorus-doped TiO_2-B nanowire arrays boosting robust pseudocapacitive properties for lithium storage. *J. Power Sources* **2018**, 396, 327–334.

(35) Yin, J.; Yu, J.; Shi, X.; Kong, W.; Zhou, Z.; Man, J.; Sun, J.; Wen, Z. TiO_2 quantum dots confined in 3*D* carbon framework for outstanding surface lithium storage with improved kinetics. *J. Colloid Interface Sci.* **2021**, 582, 874–882.

(36) Zukalová, M.; Kalbáč, M.; Kavan, L.; Exnar, I.; Graetzel, M. Pseudocapacitive lithium storage in TiO_2(B). *Chem. Mater.* **2005**, 17, 1248–1255.

(37) Xia, T.; Zhang, W.; Wang, Z.; Zhang, Y.; Song, X.; Murowchick, J.; Battaglia, V.; Liu, G.; Chen, X. Amorphous carbon-coated TiO_2 nanocrystals for improved lithium-ion battery and photocatalytic performance. *Nano Energy* **2014**, 6, 109–118.

(38) Lin, X.; Wang, Y.; Chai, W.; Liu, T.; Mou, J.; Liu, J.; Huang, J.; Liu, M. Solvothermal alcoholysis synthesis of hierarchically porous TiO_2-carbon tubular composites as high-performance anodes for lithium-ion batteries. *Electrochim. Acta* **2019**, 308, 253–262.

(39) John, W.; Julien, P.; James, L.; Bruce, D. Pseudocapacitive contributions to electrochemical energy storage in TiO_2 (anatase) nanoparticles. *J. Phys. Chem. C* **2007**, 111, 14925–14931.

(40) Torsten, B.; John, W.; Julien, P.; Bruce, D.; Sarah, H. T. Templated nanocrystal-based porous TiO_2 films for next-generation electrochemical capacitors. *J. Am. Chem. Soc.* **2009**, 131, 1802–1809.

(41) Veronica, A.; Jérémy, C.; Michael A, L.; Jong, W. K.; Pierre-Louis, T.; Sarah H, T.; Héctor D, A.; Patrice, S.; Bruce, D. High-rate electrochemical energy storage through Li^+ intercalation pseudocapacitance. *Nat. Mater.* **2013**, 12, 518–522.